Plant Communications
Resource article

CellPress
Partner Journal

Chemical inhibition of *Arabidopsis* PIN-FORMED auxin transporters by the anti-inflammatory drug naproxen

Jing Xia[1,4], Mengjuan Kong[1,4], Zhisen Yang[1,4], Lianghanxiao Sun[1], Yakun Peng[1], Yanbo Mao[1], Hong Wei[1], Wei Ying[1], Yongxiang Gao[1], Jiří Friml[2], Jianping Weng[1,*], Xin Liu[1,*], Linfeng Sun[1,*] and Shutang Tan[1,3,*]

[1]MOE Key Laboratory for Cellular Dynamics, Hefei National Laboratory for Physical Sciences at the Microscale, The First Affiliated Hospital of USTC, Biomedical Sciences and Health Laboratory of Anhui Province, Division of Life Sciences and Medicine, University of Science and Technology of China, Hefei 230027, China

[2]Institute of Science and Technology Austria (ISTA), Am Campus 1, 3400 Klosterneuburg, Austria

[3]Center for Advanced Interdisciplinary Science and Biomedicine of IHM, Division of Life Sciences and Medicine, University of Science and Technology of China, Hefei 230027, China

[4]These authors contributed equally to this article.

***Correspondence: Jianping Weng (wengjp@ustc.edu.cn), Xin Liu (lx023@ustc.edu.cn), Linfeng Sun (sunlf17@ustc.edu.cn), Shutang Tan (sttan@ustc.edu.cn)**

https://doi.org/10.1016/j.xplc.2023.100632

ABSTRACT

The phytohormone auxin plays central roles in many growth and developmental processes in plants. Development of chemical tools targeting the auxin pathway is useful for both plant biology and agriculture. Here we reveal that naproxen, a synthetic compound with anti-inflammatory activity in humans, acts as an auxin transport inhibitor targeting PIN-FORMED (PIN) transporters in plants. Physiological experiments indicate that exogenous naproxen treatment affects pleiotropic auxin-regulated developmental processes. Additional cellular and biochemical evidence indicates that naproxen suppresses auxin transport, specifically PIN-mediated auxin efflux. Moreover, biochemical and structural analyses confirm that naproxen binds directly to PIN1 protein via the same binding cavity as the indole-3-acetic acid substrate. Thus, by combining cellular, biochemical, and structural approaches, this study clearly establishes that naproxen is a PIN inhibitor and elucidates the underlying mechanisms. Further use of this compound may advance our understanding of the molecular mechanisms of PIN-mediated auxin transport and expand our toolkit in auxin biology and agriculture.

Key words: auxin transport, PIN, naproxen, *Arabidopsis*, NPA

Xia J., Kong M., Yang Z., Sun L., Peng Y., Mao Y., Wei H., Ying W., Gao Y., Friml J., Weng J., Liu X., Sun L., and Tan S. (2023). Chemical inhibition of *Arabidopsis* PIN-FORMED auxin transporters by the anti-inflammatory drug naproxen. Plant Comm. **4**, 100632.

INTRODUCTION

Plant growth and development require coordination of internal signals and environmental cues. The phytohormone auxin (indole-3-acetic acid [IAA]) plays fundamental roles in almost every aspect of a plant's life (Friml, 2022; Yu et al., 2022). Decades of genetic studies have established the molecular framework for auxin biosynthesis (Zhao, 2018), transport (Adamowski and Friml, 2015; Tan et al., 2021), and signaling (Lavy and Estelle, 2016; Gallei et al., 2020), which cooperate in a multitude of auxin functions.

IAA is synthesized by the TRYPTOPHAN AMINOTRANSFERASE OF ARABIDOPSIS/TRYPTOPHAN AMINOTRANSFERASE RELATED PROTEIN and YUCCA enzymes from the tryptophan precursor, and multiple modifications of IAA, such as oxidation or conjugation to amino acids, control IAA homeostasis in plants (Zhao, 2018). The nuclear and cytosolic TRANSPORT INHIBITOR RESPONSE1/AUXIN SIGNALLING F-BOX-AUXIN/IAA (AUX/IAA) pathway mediates auxin function in transcriptional regulation (Salehin et al., 2015; Lavy and Estelle, 2016) and rapid non-transcriptional responses related to root growth regulation (Li et al., 2022). On the other hand, cell-surface AUX BINDING PROTEIN1–TRANSMEMBRANE KINASE-based auxin

Published by the Plant Communications Shanghai Editorial Office in association with Cell Press, an imprint of Elsevier Inc., on behalf of CSPB and CEMPS, CAS.

perception confers rapid cellular auxin responses through global modulation of the phosphoproteome (Friml et al., 2022). Notably, directional auxin transport between cells, i.e., polar auxin transport, is the key feature of auxin action. Auxin transporters from the plasma membrane (PM)-localized PIN-FORMED (PIN) family pump auxin out of the cell, playing essential roles in polar auxin transport (Petrášek et al., 2006). PIN transporters reside unequally at the PM, and the polarity of PIN proteins determines the directionality of intercellular auxin flow, which is crucial for many patterning processes and for asymmetric growth during tropic responses (Adamowski and Friml, 2015; Tan et al., 2021; Konstantinova et al., 2022). AUX1/LIKE AUXINs are auxin importers (Marchant et al., 1999), and ABC transporters have also been reported to participate in auxin export (Serrano et al., 2013; Hao et al., 2020). Given the central roles of auxin in plant growth and development, exogenous auxin application and genetic or pharmacological manipulation of auxin action are widely used in both plant research and agriculture.

In the history of auxin research, various chemical tools have been developed, and they are important for overcoming the problem of functional redundancy in gene families (Kong et al., 2022). For example, L-kynurenine targets TRYPTOPHAN AMINOTRANSFERASE OF ARABIDOPSIS/TRYPTOPHAN AMINOTRANSFERASE RELATED PROTEIN enzymes to inhibit auxin biosynthesis *in planta* (He et al., 2011). Yucasin is an inhibitor of YUCCA family enzymes in the auxin biosynthesis pathway (Nishimura et al., 2014). Auxinole is an auxin antagonist of TRANSPORT INHIBITOR RESPONSE1/AUX SIGNALLING F-BOX-AUX/IAA-mediated auxin signaling. For auxin transport, there is a family of auxin transport inhibitors (ATIs), among which N-1-naphthylphthalamic acid (NPA) is widely used (Teale and Palme, 2018). Application of NPA to plants leads to various defects (e.g., interference with phototropism and gravitropism, inhibition of lateral root formation, suppression of vascular development, and deficiency in shoot development) due to suppression of auxin transport across cells (Okada et al., 1991; Gälweiler et al., 1998). NPA is also used as an herbicide at high concentrations. Recent biochemical and structural studies have revealed that NPA binds directly to and inhibits the activity of PIN auxin transporters (Abas et al., 2021; Teale et al., 2021; Lam Ung et al., 2022; Su et al., 2022; Yang et al., 2022). Interestingly, NPA binds to the same pocket as the natural PIN substrate IAA (Lam Ung et al., 2022; Su et al., 2022; Yang et al., 2022), suggesting that NPA is a competitive inhibitor of PIN proteins, which is a paradigm shift in our understanding of NPA action. Thus, identification of novel PIN inhibitors will be useful in both plant biology and agriculture.

Non-steroidal anti-inflammatory drugs (NSAIDs) such as aspirin and ibuprofen are a set of compounds used to relieve pain and fever in humans (Huls et al., 2003; Duggan et al., 2011). Among NSAIDs, salicylic acid (SA) is an ancient drug, and its use in reducing pain and fever can be traced back to the era of Hippocrates. Indeed, SA is an immune signal perceived by NON-TRANSCRIPTION OF PR GENES family receptors to regulate pathogen responses in plants (Fu et al., 2012; Wu et al., 2012; Ding et al., 2018; Wang et al., 2020). Recent studies show that SA also regulates plant growth and development (Du et al., 2013; Rong et al., 2016; Pasternak et al., 2019; Ke et al., 2021) by modulating clathrin-mediated endocytosis (Du et al., 2013) and/or targeting the A subunits of protein phosphatase 2A (Tan et al., 2020b). Oxicam-type NSAIDs have been reported to target the NON-TRANSCRIPTION OF PR GENES1 protein-mediated immune pathway as antagonists of SA in plants (Ishihama et al., 2021). Naproxen was found to inhibit abscisic acid (ABA) biosynthesis by inhibiting lipoxygenases (Creelman et al., 1992; Chernys and Zeevaart, 2000; Hansen and Grossmann, 2000). Our previous studies showed that synthetic NSAIDs had activity in plant cells (Tan et al., 2020c). Notably, among other NSAIDs, meclofenamic acid and flufenamic acid target the immunophilin-like protein TWISTED DWARF1 (TWD1; also called FKBP42) to regulate actin cytoskeletal dynamics and subsequent endomembrane trafficking (Tan et al., 2020c). Nonetheless, not all NSAIDs were found to bind the FKBP domain of TWD1 in surface plasmon resonance (SPR) assays, and how the other NSAIDs are involved in regulation of plant growth and development is unclear.

In this article, we reveal that naproxen ((S)-(+)-6-methoxy-α-methyl-2-naphthaleneacetic acid; Supplemental Figure 1A), a common NSAID that has been used for decades, exhibits typical ATI activity. Biochemical and structural experiments reveal that naproxen binds directly to the *Arabidopsis* PIN1 auxin transporter (as well as other PIN members) and inhibits its activity. Therefore, naproxen is a novel ATI, with the potential for use in both auxin research and agriculture.

RESULTS

Naproxen treatment modulates *Arabidopsis* seedling growth and development

NSAIDs, represented by aspirin and ibuprofen, are widely used to treat various aches and inflammations (Huls et al., 2003; Yiannakopoulou, 2013). In our previous study (Tan et al., 2020c), we showed that NSAIDs share bioactivities in plant cells. Among other NSAIDs, meclofenamic acid (Meclo) and flufenamic acid (Fluf) targeted TWD1 immunophilin-like protein to modulate the dynamics of actin filaments and endomembrane trafficking, thus regulating PIN2 protein trafficking to shape root growth and development in *Arabidopsis*. To further verify the molecular mechanisms that underlie the functions of other NSAIDs in plants, we focused here on naproxen and examined its physiological effects in detail. Naproxen is widely used as an anti-inflammatory drug to relieve pain and swelling by inhibiting the cyclooxygenase-2- enzyme to reduce prostaglandin production in animal cells (Duggan et al., 2010).

When grown on Murashige and Skoog (MS) plates supplemented with naproxen (10, 20, and 40 μM, respectively), *Arabidopsis* seedlings exhibit shorter (Figures 1A and 1B) and less gravitropic primary roots (Figures 1A and 1D and Supplemental Figure 1C), as well as a reduced number of lateral roots compared with those in the DMSO control (Figure 1C and Supplemental Figure 1B) (Tan et al., 2020c). To further test the effect of naproxen on root gravitropism, *Arabidopsis* Columbia-0 (Col-0) seedlings were gravistimulated by 90° reorientation, and as expected, roots bent down toward gravity in the DMSO control. By contrast, roots grew in random directions under naproxen treatment, suggesting an impaired gravitropic response (Supplemental Figures 2A and 2B). These effects of

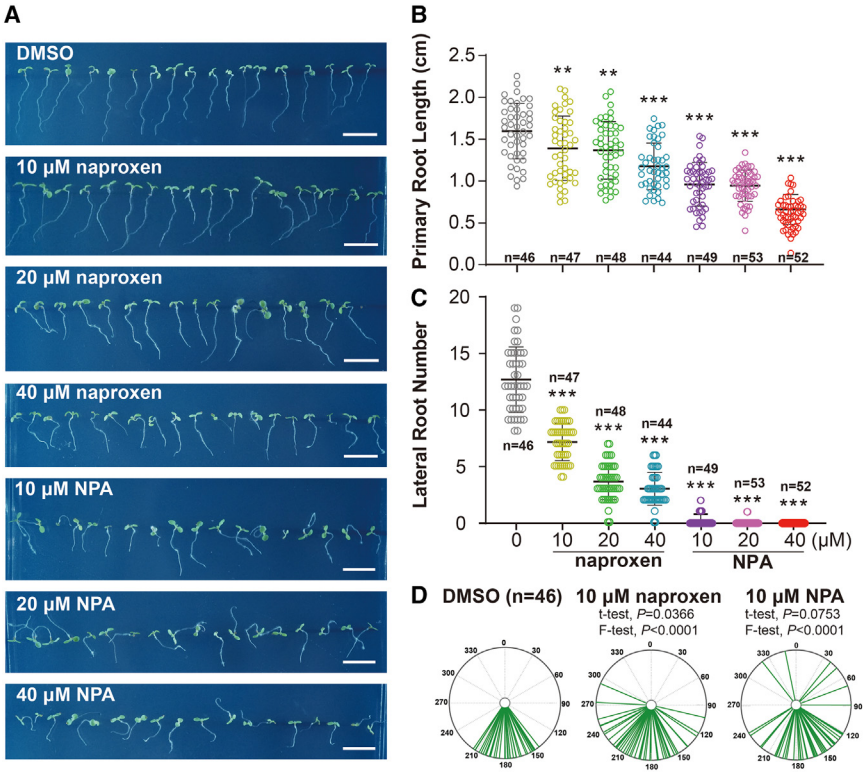

Figure 1. Physiological effects of naproxen on *Arabidopsis* root development.

(A) Representative images showing morphological changes in roots of 7-day-old Col-0 seedlings grown on MS medium supplemented with naproxen and NPA at the indicated concentrations. DMSO was used as the solvent control. Scale bars, 1 cm.

(B and C) Dose-dependent inhibitory effect of naproxen and NPA on primary root elongation in 7-day-old Col-0 seedlings. Naproxen and NPA suppressed lateral root formation. The emerged lateral roots of 10-day-old Col-0 seedlings treated with naproxen and NPA were counted. *p* values were calculated by comparing different treatments to DMSO using an unpaired *t*-test with Welch's correction. $^{**}p < 0.01$, $^{***}p < 0.001$.

(D) Naproxen and NPA interfered with root gravitropism. 7-day-old Col-0 seedlings were grown on MS medium supplemented with DMSO, naproxen, or NPA, as indicated. Each line represents the root tip angle of an individual seedling in polar charts. Unpaired *t*-tests indicate significant differences among means, and F-tests indicate significant differences among variances. DMSO is the solvent control, and NPA is the positive control.

naproxen on root development are reminiscent of NPA, a widely used ATI (Tan, 2021; Kong et al., 2022). We therefore explored the activities of naproxen, with NPA as a control, in auxin transport-dependent biological processes in more detail.

Auxin plays a central role in plant tropic responses toward gravity and light, i.e., gravitropism and phototropism. For both processes, PIN-mediated polar auxin transport determines the asymmetric (re)distribution of this growth hormone, thus ensuring differential growth of plant organs (Friml et al., 2002; Ding et al., 2011; Rakusová et al., 2016). When wild-type Col-0 *Arabidopsis* seedlings were grown on MS medium with the DMSO solvent control in the dark, they grew upright, whereas seedlings on MS plates with naproxen were less gravitropic (Supplemental Figures 3A, 3C, and 3D). Upon gravistimulation by 90° rotation, seedlings bent upward on MS medium with the DMSO control, whereas those on naproxen showed less bending, suggesting a defect in either gravity perception or gravity-stimulated differential growth (Supplemental Figures 3B and 3E). To confirm these findings, 4-day-old etiolated seedlings were transferred to plates with DMSO, naproxen, or NPA; after 24 h of gravistimulation, seedlings bent upward on the DMSO control, bent to a lesser extent on naproxen, and had lost gravitropism on NPA (Supplemental Figures 4A and 4B). Notably, NPA impaired apical hook formation, which requires polar auxin transport (Vandenbussche et al., 2010; Zadnikova et al., 2010), whereas naproxen showed a much smaller effect at the tested concentrations (Supplemental Figures 3A and 3B), suggesting a different mode of action for this process. Similarly, naproxen also compromised phototropism of *Arabidopsis* seedlings (Supplemental Figure 5). These results suggest that naproxen impaired numerous processes in auxin-mediated plant growth and development, albeit with less specificity and potency than the traditional ATI NPA.

Naproxen interferes with auxin response *in planta*

To test whether naproxen interferes with the auxin pathway, we used the *DR5rev::GFP* auxin-responsive reporter, which is used to indicate auxin distribution or signaling (Friml et al., 2003). Auxin forms a regular maxima at the root tip, which is important for root meristem patterning and gravitropic response (Adamowski and Friml, 2015). Decreased activity of PIN transporters in mutants of the responsible activating kinases such as *d6pk d6pkl1 d6pkl2* and *pdk1.1 pdk1.2* caused an expansion of root tips with an enlarged DR5 region due to overproliferation of columella cells (Tan et al., 2020a; Xiao and Offringa, 2020). A similar phenomenon was also observed in NPA-treated roots, with a broader DR5 signal (Figure 2A). Intriguingly, naproxen exerts the same effect, although at a higher concentration (40 μM) than NPA (10 μM) (Figure 2A). This constitutive treatment also led to tissue swelling in root tips with overgrowth of gravity-sensing columella cells (statocytes), as revealed by Lugol staining (Figure 2B). The overproliferation of statocytes was correlated with the DR5 pattern, which was reported to be due to exaggeration of the region with auxin maxima (Nakamura et al., 2019). The similar activities of NPA and naproxen prompted us to test whether naproxen functions in a similar way. Notably, the effects of naproxen were not identical to those of NPA regardless of dosage, suggesting the existence of potential additional targets for naproxen.

In the gravitropic response, auxin (as monitored by DR5) redistributes and accumulates at the lower side of the root, where it

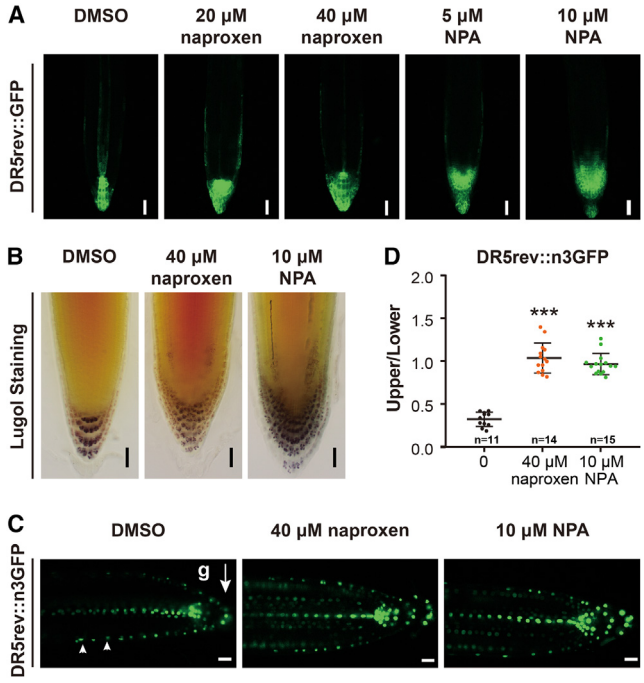

Figure 2. Naproxen interferes with auxin response *in planta*.

(A) The regular auxin-responsive pattern of *DR5rev::GFP* was disrupted by naproxen and NPA treatments. 5-day-old *DR5rev::GFP* seedlings grown on MS plates containing naproxen or NPA at the indicated concentrations were imaged by confocal laser scanning microscopy, n = 12–16, and scale bars, 50 μm.

(B) Constant naproxen and NPA treatments changed the pattern of statocytes. 5-day-old Col-0 seedlings from the indicated treatments were stained with Lugol solution and imaged with a differential interference contrast microscope, n = 15–20, and scale bars, 20 μm.

(C and D) Naproxen and NPA treatments suppressed the DR5revn3GFP redistribution pattern under gravistimulation. 5-day-old *DR5v2::ntdTomato;DR5rev::n3GFP* seedlings grown on normal plates were transferred to DMSO/naproxen/NPA-containing plates and rotated by 90° for an additional 4 h. Root tips were imaged by confocal laser scanning microscopy for the GFP channel.

(C) Representative images. The arrowhead indicates the direction of gravity. Scale bars, 20 μm.

(D) The upper:lower ratio for the DR5 signal was measured to indicate relocation. p values were calculated by comparing different treatments with the DMSO control using an unpaired *t*-test with Welch's correction, $^{***}p < 0.001$.

inhibits cell elongation to promote downward bending (Baster et al., 2013). As expected, naproxen treatment impaired the seedlings' ability to respond to gravistimulation (Supplemental Figures 2A and 2B), and this was accompanied by a defect in asymmetric DR5 signal formation (Figures 2C and 2D), suggesting that naproxen may interfere with polar auxin transport from root tips during the gravitropic response. Taken together, these results indicate that naproxen may inhibit auxin transport in plant cells.

Naproxen inhibits auxin transport by binding directly to PIN proteins

The physiological and cellular analyses above suggest that naproxen may be an ATI. Using an auxin efflux assay based on HEK293F cells and purified PIN1 protein (Yang et al., 2022), we tested whether naproxen targets PIN auxin transporters directly. In the auxin efflux assay, which measured residual ^{3}H-labeled radioactive IAA ([^{3}H]-IAA) in cells after transfer to isotope-free buffer, cells that expressed PIN1 plus the activating kinase D6PK (i.e., the PIN1 group) had much lower retention of [^{3}H]-IAA than cells transfected with the empty vector (the control group), suggesting that auxin efflux was mediated by PIN1 protein (Figure 3A). NPA or naproxen treatment of cells expressing PIN1 plus D6PK led to retention of [^{3}H]-IAA similar to that in the control group but higher than that in untreated cells, suggesting strong inhibition of auxin export by NPA or naproxen at a concentration of 50 μM (Figure 3A). This result implies that naproxen may target PIN1 protein directly.

To further test this hypothesis, we measured the binding between PIN1 prepared in detergent micelles and naproxen using a surface plasmon resonance (SPR) assay, and the results indicated that naproxen indeed bound to PIN1 protein, with a kinetic dissociation constant (K_D) value of approximately 12.4 μM (Figures 3B and 3C). The binding between PIN1 and naproxen was also validated by an isothermal titration calorimetry (ITC) assay. The PIN1 protein was prepared with the amphiphilic polymer amphipol (A8-35) to preclude possible impacts of the detergent micelles. Again, clear binding was observed between PIN1 and naproxen, with a K_D value of 3.14 ± 0.62 μM (Supplemental Figure 6A), which is within a range similar to that detected by SPR. It is noteworthy that naproxen had a lower binding affinity to PIN1 protein than did NPA, whose K_D value was 0.0166 μM, as also revealed by SPR (Supplemental Figures 6B and 6C). This correlates well with the physiological and cellular experiments in which naproxen exhibited lower activity than NPA. This can be explained by the structures of NPA-bound and naproxen-bound PIN1 complexes, as NPA is bulkier than naproxen. Although both compounds contain a carboxyl group that forms hydrogen bonds with PIN1, NPA has a benzene ring that forms hydrophobic stackings with the surrounding residues (Yang et al., 2022). However, in naproxen, this ring is replaced by a smaller methyl group. We also tested the binding affinity between naproxen and other PINs (PIN2, PIN5, and PIN8) using SPR, and naproxen bound to all PINs examined with K_D values similar to that of naproxen–PIN1 (Supplemental Figures 6D–6H).

Structural basis for naproxen inhibition of PIN-mediated auxin transport

To gain insight into the inhibition mechanism of naproxen, we tried to determine the complex structure of PIN1 and naproxen. Naproxen was added to purified PIN1 protein bound with the synthetic nanobody sybody-19 (Yang et al., 2022) prior to cryo-sample preparation. After cryoelectron microscopy (cryo-EM) data collection and processing, an EM map with an overall resolution of 3.7 Å was obtained (Figure 4A and Supplemental Figures 7A–7F and 8A). The overall EM density was similar to those of previously determined PIN1 structures. In the intracellular cavity, a clear density was observed that docked well with naproxen (Figures 4A and 4B and Supplemental Figure 8B). Such a cavity has also been shown to accommodate the natural auxin IAA and the inhibitor NPA (Yang et al., 2022). In line with the higher binding affinity of naproxen to PIN1 protein (with a K_D value of 12.4 μM; Figures 3B and 3C) than to IAA (with a K_D value of 186 μM, as

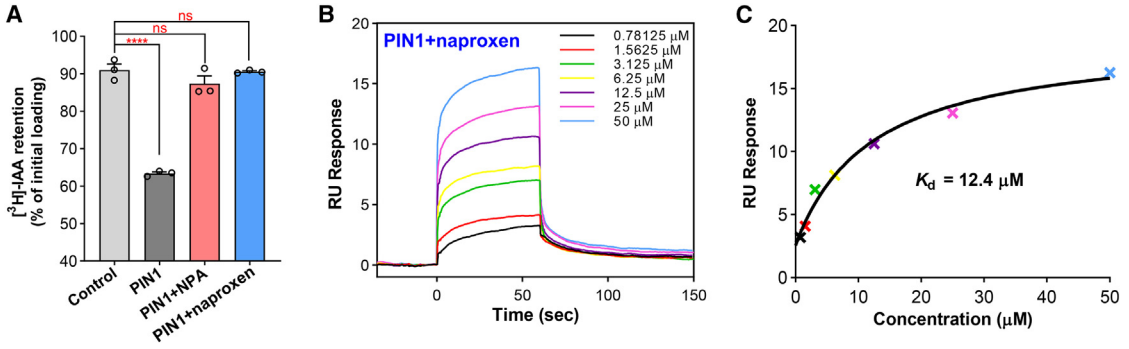

Figure 3. Naproxen binds to and inhibits the auxin efflux activity of PIN1.

(A) [^{3}H]IAA retention relative to initial loading in the absence or presence of 50 μM NPA or 50 μM naproxen. Each data point is the average of three independent experiments. Statistical analysis was performed using one-way ANOVA with Dunnett's multiple comparisons test. ns, not significant, ****$p <$ 0.0001 for wild type versus control. Data are presented as mean ± SEM.

(B) SPR signals for the association and dissociation of naproxen with PIN1. RU, resonance units.

(C) Data from **(B)** were analyzed with a steady-state affinity binding model. The resulting dissociation constant (K_D) was determined to be 12.4 μM.

determined by SPR in Yang et al. [2022]), this result suggests that naproxen functions as a competitive inhibitor of IAA for PIN transporters.

This complex structure aligns well with apo-state PIN1, the NPA-bound structure of PIN1, and the IAA-bound structure of PIN1, with root-mean-square deviations of 0.50, 0.53, and 0.95 Å, respectively, all of which exhibit an inward-facing conformation (Supplemental Figures 7G–7I; Supplemental Video 1). Like NPA, naproxen binds to PIN1 through both hydrogen bonding and hydrophobic interactions (Figures 4C and 4D). The carboxyl group of naproxen lies between N112 and Y145 and forms a hydrogen bond with Y145. The naphthalene moiety is stacked between hydrophobic residues of PIN1, including V51, V115, I582, and V583 (Figures 4C and 4D). This suggests a conserved binding mode of naproxen and NPA with PIN1, which is also reflected in the well-superposed binding sites of the structures (Figure 4E). However, the carboxyl group of NPA forms more hydrogen bonds with PIN1, as with the backbones of I582 and V583, and the benzene ring also forms hydrophobic stacking with Y145, L114, and V583 (Yang et al., 2022), which may contribute to the higher binding affinity of NPA with PIN1. Notably, these amino acid residues are conserved in PM-localized PIN proteins but vary in ER-localized PINs (Yang et al., 2022). Although SPR assays suggest that naproxen also binds to PIN5 and PIN8 proteins, the detailed mechanism requires further structural analyses.

To verify the functions of these amino acid residues around the binding pockets of IAA (Yang et al., 2022) and naproxen, we generated V51A, K472A, N478A, D512A, R547A, Q580A, and I582A point mutants and transformed their GFP-fused versions driven by the native PIN1 promoter into the loss-of-function *pin1-613* mutant. Phenotypic analysis revealed that none of these mutated versions of PIN1–GFP could rescue the inflorescence defects of *pin1-613* compared with the wild-type *PIN1* transgene (Supplemental Figure 9A). Notably, these mutated versions of PIN1–GFP exhibited a basal subcellular localization at the PM in root stele cells, similar to that of the wild-type PIN1 protein (Supplemental Figure 9B), confirming that these amino acid residues are required for PIN1 activity but do not affect PIN1 polarity (Yang et al., 2022). Together with that fact that the binding affinity for naproxen–PIN1 (with a K_D value of 12.4 μM in the SPR assay) is higher than that of IAA-PIN1 (with a K_D value of 186 μM), binding of naproxen to these key amino acid residues for IAA association may explain the mechanism by which naproxen inhibits auxin transport.

DISCUSSION

Auxin plays essential roles in plant growth and development. Synthetic auxins and anti-auxin compounds are important tools in both plant research and modern agriculture. Among these chemicals, ATIs have been used as herbicides in agriculture. In this study, we revealed that naproxen is a novel ATI that directly targets PIN auxin transporters. Naproxen treatment produces a variety of morphogenetic changes in *Arabidopsis* seedlings that can be ascribed to disturbance in auxin distribution. The effects of naproxen in plants are reminiscent of those of *pin* mutants, such as shortened root length in *pin1 pin3 pin4* or *pin1 pin3 pin4 pin7* (Friml et al., 2003), lateral root deficiency in *pin1* (Benková et al., 2003), agravitropic roots in *pin2* (Chen et al., 1998; Luschnig et al., 1998) or *pin3* (Kleine-Vehn et al., 2010), agravitropic hypocotyls in *pin3 pin4 pin7* etiolated seedlings (Rakusová et al., 2016), and impaired phototropism in *pin3* or *pin3 pin4 pin7* mutants (Friml et al., 2002; Ding et al., 2011). Indeed, a high concentration of naproxen markedly suppressed plant growth, similar to NPA (Supplemental Figures 10A and 10B). Biochemical and structural analyses confirmed that naproxen binds directly to the IAA-binding pocket of PIN1 protein. Intriguingly, although the binding profiles of NPA and naproxen are quite similar, there are still differences in their detailed interactions and binding affinities, suggesting the potential for further engineering to develop novel compounds that target PIN transporters.

We used purified PIN1 protein (Yang et al., 2022) to perform the transport assays and structural analysis. However, given that naproxen exhibits broader ATI activities *in planta* than targeting PIN1 alone and that the active sites are conserved across PIN family auxin transporters, naproxen may target other PIN homologs in the same manner, as supported by the SPR

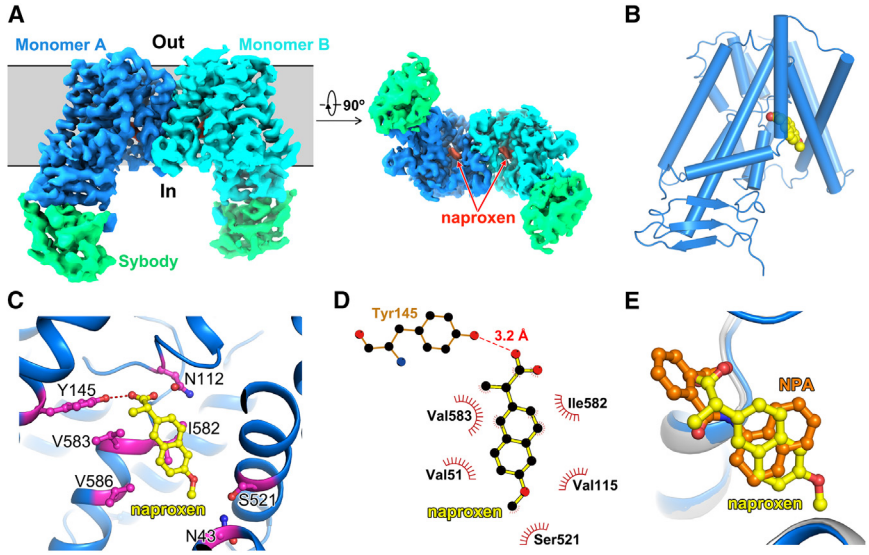

Figure 4. Structure of naproxen-bound PIN1.

(A) Overall cryo-EM map of PIN1 in complex with naproxen. Densities of the two protomers are shown in blue (monomer A) and cyan (monomer B). The sybodies are colored green. Naproxen (red density) in the map of each PIN1 subunit is indicated with red arrows. Side view and bottom view are presented.

(B) Cartoon representation of PIN1 monomer–bound naproxen. Naproxen is shown as spheres. The structure of naproxen-bound PIN1 exhibits an inward-facing conformation.

(C) Coordination of naproxen by PIN1. Naproxen and interacting residues are shown by sticks. Hydrogen bonds are shown as red dashed lines.

(D) Schematic representation of naproxen–PIN1 interactions as shown by Ligplot$^+$ (red dashed line, hydrogen bond; spokes, hydrophobic interactions).

(E) Superposition of the naproxen-bound and NPA-bound (PDB: 7Y9U) structures of PIN1. Naproxen and NPA are shown by yellow and orange sticks, respectively.

results (Supplemental Figures 6C–6I). Naproxen was reported to inhibit ABA biosynthesis by suppressing lipoxygenase activity in plants (Creelman et al., 1992; Chernys and Zeevaart, 2000; Hansen and Grossmann, 2000); however, whether this ABA pathway is involved in the auxin-related effects reported here and whether naproxen also targets other proteins *in planta* require further investigation. Moreover, as we have noticed that other NSAIDs, such as indomethacin and ketoprofen, also exhibit activities (i.e., causing overproliferation of root columella cells and expansion of the DR5 signal) similar to those of naproxen and NPA (Tan et al., 2020c), it is likely that more NSAIDs also target PIN proteins. Previously, we reported that meclofenamic acid and flufenamic acid target TWD1 to regulate the dynamics of the actin cytoskeleton (Tan et al., 2020c), suggesting that NSAIDs may have diverse cellular effects. Although a high concentration of naproxen (100 μM) also has effects on actin cytoskeletal dynamics and vesicle trafficking, its binding to TWD1 was undetectable in our previous study (Tan et al., 2020c), suggesting potentially different regulatory mechanisms. Further exploration of the NSAID family and their *in vivo* targets may advance our understanding of their bioactivities.

METHODS

Plant materials and growth conditions

Arabidopsis thaliana (L.) lines used in this study were in the Col-0 ecotype background. The *pin1-613* (SALK_047613) mutant was reported previously. The marker lines *DR5rev::GFP* (Friml et al., 2003) and *DR5v2::tdTomato;DR5rev::n3GFP* (Liao et al., 2015) were described previously.

For the *pin1*;*PIN1-mGFP4* point mutant transgenic lines driven by the PIN1 promoter, a *PIN1-mGFP4* sequence was first amplified from the genomic sequence of the *pPIN1::PIN1-GFP* reporter line (Benková et al., 2003) and subcloned into a pDONR221 vector. Point-mutated versions of PIN1 were generated with a kit (primers are listed in Supplemental Table 1) in the pDONR221–PIN1–mGFP4 plasmid. The resultant constructs were cloned into a pB7m24GW,3 destination vector together with a pDONR–P4P1r–pPIN1 plasmid. The floral dip method (Clough and Bent, 1998) was used for transformation into the *pin1-613*$^{+/-}$ background. T_2 generation plants in the *pin1-613* homozygous background were used for phenotyping analysis after genotyping.

For phenotyping of seedlings or pharmacological experiments, seeds were surface sterilized with 75% ethanol and sown on 0.5× MS medium supplemented with 1% (w/v) sucrose and 0.8% (w/v) phytoagar (pH 5.9), stratified at 4°C for 2 days, and then grown in a growth chamber at 21°C with a long-day photoperiod (16 h light/8 h dark). For the dark treatment, the plates were covered with aluminum foil. For the phototropic response assay, 4-day-old etiolated seedlings were exposed to light for 6 h and then exposed to a directional light source (compact fluorescent lamp, Philips). For microscopy analysis, 5-day-old seedlings of different reporter lines were treated with naproxen and NPA on MS plates.

Pharmacological treatments

For pharmacological treatments, *Arabidopsis* seeds were sown on MS plates with the indicated chemicals, including naproxen (Sigma, N8280), naproxen sodium (Sigma, M1275, used for high concentration in the growth assays in Supplemental Figure 10 and in the binding assays), and NPA (Sigma, N12507). After stratification for 2 days at 4°C, the plates were transferred to a growth chamber under the conditions described in the plant materials and growth conditions section for 5, 7, or 10 days depending on the assay. The phenotype was then analyzed using confocal laser scanning microscopy (CLSM) or ImageJ.

For short-term treatment to study the subcellular localization of *DR5v2::ntdTomato;DR5rev::n3GFP*, seedlings (aged 5 days) grown on normal MS plates were transferred to MS plates containing DMSO/naproxen/NPA and rotated by 90° for 4 h. Afterward, the samples were imaged using CLSM.

CLSM imaging

Fluorescence imaging was performed using a Zeiss LSM 980 CLSM equipped with a GaAsP detector (Zeiss). The manufacturer's default settings (smart mode) were used to image proteins tagged with GFP (excitation, 488 nm; emission, 495–545 nm). All images were obtained in 8-bit depth with 2× line averaging. Images were analyzed with ImageJ software (NIH).

Statolith starch staining using Lugol solution

Five-day-old *Arabidopsis* Col-0 seedlings treated with naproxen and NPA (with DMSO as the solvent control) were stained with Lugol solution for 2 min and then washed with liquid MS medium for 2 min. The samples were mounted with a clearing solution (30 ml H_2O, 10 ml glycerol, 80 g chloral hydrate in a total volume of 100 ml). Finally, root tips were imaged using a differential interference contrast microscope (Olympus BX53).

Imaging and morphological analysis of *Arabidopsis* seedlings

For physiological experiments, MS plates with *Arabidopsis* seedlings were imaged using a Sony A6000 camera with a macro lens, and primary root length, root tip angles, hypocotyl length, or growth direction were analyzed with ImageJ software (NIH). Lateral root numbers were counted directly. Apical hooks of etiolated seedlings were imaged using a stereomicroscope (Nikon, SMZ1500).

Protein expression and purification

Protein purification was performed as described previously (Yang et al., 2022). The DNA sequences of full-length *Arabidopsis thaliana PIN1*, *PIN2*, *PIN5*, and *PIN8* were subcloned into the pCAG vector (Invitrogen) with the N-terminal FLAG tag (primers are listed in Supplemental Table 1). The HEK 293F cells (Sino Biological) were cultured in SMM 293T-II medium (Sino Biological) at 37°C supplemented with 5% CO_2. 1.5 mg plasmids and 4 mg linear polyethylenimine (Polysciences) were pre-incubated in 50 ml fresh medium for 30 min before being added to one liter (l) of cells at a density of 3×10^6 cells ml^{-1}. Then the mixture was added to the cell culture, followed by 15 min incubation. The transfected cells were collected after 60 h culture and resuspended in lysis buffer containing 25 mM HEPES (pH 7.4) and 150 mM NaCl supplemented with 1.3 mg ml^{-1} aprotinin, 5 mg ml^{-1} leupeptin, 0.7 mg ml^{-1} pepstatin, and 1 mM phenylmethylsulfonyl fluoride. Then, the suspension was incubated in the buffer with an additional 1.5% (w/v) n-dodecyl-β-D-maltopyranoside (Anatrace) at 4°C for 2 h. After centrifugation at 14 000 rpm for 60 min, the supernatant was incubated with anti-FLAG M2 affinity gel (Sigma) at 4°C for 45 min. The resin was rinsed 3 times with 10 ml buffer (25 mM HEPES [pH 7.4], 150 mM NaCl, 0.06% (w/v) glyco-diosgenin [Anatrace]). The protein was eluted with wash buffer plus 200 μg/ml FLAG peptide. To prepare PIN1 and the sybody (sybody-21 used for final structure determination) complex, purified PIN1 and sybody-19 were mixed together in a molar ratio of ∼1:3 and then subjected to size-exclusion chromatography using a Superose 6 Increase column (GE Healthcare) in buffer containing 25 mM HEPES (pH 7.4), 150 mM NaCl, and 0.02% (v/v) glyco-diosgenin. Peak fractions were pooled and concentrated to approximately 6 mg ml^{-1} for structural studies.

For the ITC assay, PIN1 was reconstituted in the polymer amphipols. Purified PIN1 was mixed with amphipols A8–35 (Anatrace) at a 1:3 (w/w) ratio with gentle agitation for 4 h. Detergent was removed by incubation with Bio-Beads SM-2 (Bio-Rad) at 4°C overnight. Free amphipol molecules were removed with a Superose 6 Increase column in buffer containing 25 mM HEPES (pH 7.4) and 150 mM NaCl. Peak fractions were collected for further analysis.

Sample preparation and cryo-EM data acquisition

To prepare naproxen-bound PIN1 cryo-EM samples, 1 mM naproxen was incubated with the protein on ice for 1 h, and then a 4-μl sample was applied to a glow-discharged holey carbon grid (Quantifoil Cu R1.2/1.3, 300 mesh). The grid was blotted for 4 s and then plunged into liquid ethane using a Vitrobot Mark IV (FEI) at 8°C and 100% humidity. The dataset was collected on a 300 kV Titan Krios cryo-EM (Thermo Fisher Scientific) with a nominal magnification of 81 000×. Images were recorded by a K3 direct electron detector positioned after a quantum energy filter (Gatan) in super-resolution mode with a pixel size of 0.55 Å by EPU software (Thermo Fisher Scientific). A total of 2414 images were collected with defocus values varying from −1.5 to −2.3 μm. Each image was acquired with an exposure time of 3 s and dose fractionated to 32 frames with a total dose of 50 e^- $Å^{-2}$.

Image processing for cryo-EM data

The data processing workflow is presented in Supplemental Figure 7F. All micrographs were first imported into Relion 3.1 for image processing (Zivanov et al., 2018). The beam-induced motion correction and dose weighting were performed using MotionCor2 (Zheng et al., 2017). Micrographs were then imported into cryoSPARC for all subsequent image processing tasks (Punjani et al., 2017). Contrast transfer function estimates were obtained with implemented patch contrast transfer function. For the structure analysis, 1 157 541 particles were automatically picked for 2D classification; 365 141 particles were selected after 2D classification and then subjected to *ab initio* 3D classification into five classes. The best class was selected for non-uniform refinement, and a map at 4.2 Å was obtained. Further *ab initio* reconstructions and heterorefinement were performed to improve the resolution. The final 3D cryo-EM density map was reconstructed and refined at 3.7 Å, as estimated with the gold-standard FSC at a 0.143 criterion with a high-resolution noise substitution method (Rosenthal and Henderson, 2003; Chen et al., 2013). Local resolution estimation was performed using cryoSPARC.

Model building

The 3.7-Å reconstruction map for naproxen-bound PIN1 was used for model building in COOT (Emsley et al., 2010). The previously solved structure of apo PIN1 (PDB: 7Y9T) was docked into the cryo-EM map using UCSF Chimera to generate the initial model. The model was then refined with iterative cycles of manual refitting in COOT (Emsley et al., 2010) and real space refined using PHENIX with secondary structure and geometry restraints (Adams et al., 2010). Statistics of the 3D reconstruction and model refinement can be found in Supplemental Table 2.

Surface plasmon resonance

The SPR analysis was performed using a Biacore 8K system (Cytiva) at 25°C with a flow rate of 30 μl min^{-1}. Purified wild-type PIN1, PIN2, PIN5, or PIN8 proteins were immobilized onto the series S CM5 sensor chips (Cytiva) by amine-coupling chemistry. The bound protein in the chip was 23 686 resonance units (RUs) for PIN1, 27 660 RUs for PIN2, 26 837 RUs for PIN5, and 26 892 RUs for PIN8. NPA or naproxen at different concentrations was flowed over the chip surface in running buffer (pH 7) consisting of 25 mM HEPES (pH 7), 150 mM NaCl, surfactant P20, and 5% (v/v) DMSO. Data were analyzed with Biacore Insight Evaluation Software v.3.0.12 using a steady-state affinity binding model.

ITC

The binding affinity between naproxen and PIN1 in amphipol was measured with a MicroCal iTC200 microcalorimeter (MicroCal). Purified PIN1 protein in buffer containing 25 mM HEPES (pH 7.4) and 150 mM NaCl was concentrated to about 0.035 mM. The protein was titrated with 1 mM naproxen sodium salt (to avoid the potential effects of pH changes) dissolved in an identical buffer at 25°C. Binding isotherms were plotted, analyzed, and fitted based on a one-set-of-sites binding model using MicroCal PEAQ-ITC Analysis software (Malvern Panalytical).

Cell-based auxin efflux assays

Auxin efflux assays followed a general protocol reported previously (Yang et al., 2022). In brief, PIN1 and *A. thaliana* D6PK (UniProt: Q9FG74) were subcloned into the pCAG vector. HEK 293F cells at a density of 1.5×10^6 cells ml^{-1} were cotransfected with PIN1 or the empty vector and D6PK at a mass ratio of 3:1. After 24 h transfection, cells were harvested by centrifugation and resuspended in buffer consisting of PBS citrate buffer (pH 5.5; 10 mM Na_2HPO_4, 1.8 mM KH_2PO_4, 2.7 mM KCl, 137 mM NaCl, pH adjusted with anhydrous citric acid) and 50 μM NPA (Sigma) or naproxen for 5 min, with DMSO as the control. Cells were then loaded in PBS citrate buffer (pH 5.5) with 40 nM [^{3}H]IAA (specific activity 25 Ci $mmol^{-1}$, American Radiolabeled Chemicals) and 50 μM inhibitors. After 5 min incubation, cells were washed by centrifugation and resuspended in [^{3}H]-IAA-free PBS citrate buffer. A 500-μl aliquot of cell suspension containing 3×10^6 cells was taken immediately after resuspension (defined as the zero time point) and at 10-min time points. Cells were centrifuged and washed twice with 1 ml ice-cold PBS buffer (pH 7.4) and resuspended with the same buffer plus 1% (v/v) Triton X-100. Finally, 2 ml scintillation fluid was added for scintillation counting. The radioactivity in cell extracts was counted by liquid scintillation

counting (Tri-Carb 2910TR, PerkinElmer). [^{3}H]IAA retention is presented as residual radioactivity measured at 10 min relative to that at 0 min. All experiments were repeated independently three times.

Quantification and statistics

Most experiments were repeated independently at least three times with similar results. To measure hypocotyl length, primary root length, root tip angles, apical hooks, and hypocotyl growth direction, photographs were analyzed using ImageJ (https://imagej.nih.gov/ij/download.html). Fluorescence intensity of CLSM images was quantified by Fiji (https://fiji.sc/). Data visualization and statistics were performed mainly with GraphPad Prism 8. For bending curvatures of roots or hypocotyls, polar bar graphs were generated with Origin (2021).

DATA AVAILABILITY

The 3D cryo-EM density map of naproxen-bound AtPIN1 has been deposited in the Electron Microscopy Data Bank (https://www.ebi.ac.uk/emdb/) under accession number EMD-36254. Coordinates for the naproxen-bound structure model have been deposited in the PDB (https://www.rcsb.org/) under accession code 8JH5. All data necessary to evaluate the conclusions of the paper and the supplemental information are available from the corresponding authors upon request.

SUPPLEMENTAL INFORMATION

Supplemental information is available at *Plant Communications Online*.

FUNDING

This work was supported by the Strategic Priority Research Program of the Chinese Academy of Sciences (XDB37020103 to Linfeng Sun); research funds from the Center for Advanced Interdisciplinary Science and Biomedicine of IHM, Division of Life Sciences and Medicine, University of Science and Technology of China (QYPY20220012 to S.T.); start-up funding from the University of Science and Technology of China and the Chinese Academy of Sciences (GG9100007007, KY9100000026, KY9100000051, and KJ2070000079 to S.T.); the National Natural Science Foundation of China (31900885 to X.L. and 31870732 to Linfeng Sun); the Natural Science Foundation of Anhui Province (2008085MC90 to X.L. and 2008085J15 to Linfeng Sun); the Fundamental Research Funds for the Central Universities (WK9100000021 to S.T. and WK9100000031 to Linfeng Sun); and the USTC Research Funds of the Double First-Class Initiative (YD9100002016 to S.T. and YD9100002004 to Linfeng Sun). Linfeng Sun is supported by an Outstanding Young Scholar Award from the Qiu Shi Science and Technologies Foundation and a Young Scholar Award from the Cyrus Tang Foundation.

AUTHOR CONTRIBUTIONS

X.L., Linfeng Sun, and S.T. conceived the project and designed the experiments. The physiological effect of naproxen was originally discovered by S.T. in J.F.'s lab at ISTA. M.K., Lianghanxiao Sun, Y.P., and Y.M. performed physiological and cell biological experiments under the supervision of S.T. Z.Y. and J.X. performed protein purification, biochemical assays, and structure determination work under the supervision of J.W., X.L., and Linfeng Sun. Z.Y., J.X., H.W., and W.Y. performed the auxin transport assays. Z.Y. and Y.G. performed the cryo-EM data collection. All authors contributed to data analysis. J.W. and J.F. contributed to manuscript preparation. X.L., Linfeng Sun, and S.T. wrote the manuscript with input from other co-authors, and all authors revised and approved the submitted version.

ACKNOWLEDGMENTS

We thank Dr. Yang Zhao for sharing published materials (Center for Excellence in Molecular Plant Sciences, Chinese Academy of Sciences) and the Cryo-EM Center of the University of Science and Technology of China for the EM facility support. We are grateful to Y. Gao and all other staff members for their technical support on cryo-EM data collection. No conflict of interest is declared.

Received: March 17, 2023
Revised: April 12, 2023
Accepted: May 24, 2023
Published: May 29, 2023

REFERENCES

Abas, L., Kolb, M., Stadlmann, J., Janacek, D.P., Lukic, K., Schwechheimer, C., Sazanov, L.A., Mach, L., Friml, J., and Hammes, U.Z. (2021). Naphthylphthalamic acid associates with and inhibits PIN auxin transporters. Proc. Natl. Acad. Sci. USA **118**. e2020857118.

Adamowski, M., and Friml, J. (2015). PIN-dependent auxin transport: action, regulation, and evolution. Plant Cell **27**:20–32.

Adams, P.D., Afonine, P.V., Bunkóczi, G., Chen, V.B., Davis, I.W., Echols, N., Headd, J.J., Hung, L.W., Kapral, G.J., Grosse-Kunstleve, R.W., et al. (2010). PHENIX: a comprehensive Python-based system for macromolecular structure solution. Acta Crystallogr. D Biol. Crystallogr. **66**:213–221.

Baster, P., Robert, S., Kleine-Vehn, J., Vanneste, S., Kania, U., Grunewald, W., De Rybel, B., Beeckman, T., and Friml, J. (2013). SCFTIR1/AFB-auxin signalling regulates PIN vacuolar trafficking and auxin fluxes during root gravitropism. EMBO J. **32**:260–274.

Benková, E., Michniewicz, M., Sauer, M., Teichmann, T., Seifertová, D., Jürgens, G., and Friml, J. (2003). Local, efflux-dependent auxin gradients as a common module for plant organ formation. Cell **115**:591–602.

Chen, R., Hilson, P., Sedbrook, J., Rosen, E., Caspar, T., and Masson, P.H. (1998). The *Arabidopsis thaliana* AGRAVITROPIC 1 gene encodes a component of the polar-auxin-transport efflux carrier. Proc. Natl. Acad. Sci. **95**:15112–15117.

Chen, S., McMullan, G., Faruqi, A.R., Murshudov, G.N., Short, J.M., Scheres, S.H.W., and Henderson, R. (2013). High-resolution noise substitution to measure overfitting and validate resolution in 3D structure determination by single particle electron cryomicroscopy. Ultramicroscopy **135**:24–35.

Chernys, J.T., and Zeevaart, J.A. (2000). Characterization of the 9-cis-epoxycarotenoid dioxygenase gene family and the regulation of abscisic acid biosynthesis in Avocado. Plant Physiol. **124**:343–353.

Clough, S.J., and Bent, A.F. (1998). Floral dip: a simplified method for *Agrobacterium*-mediated transformation of *Arabidopsis thaliana*. Plant J. **16**:735–743.

Creelman, R.A., Bell, E., and Mullet, J.E. (1992). Involvement of a lipoxygenase-like enzyme in abscisic acid biosynthesis. Plant Physiol. **99**:1258–1260.

Ding, Z., Galván-Ampudia, C.S., Demarsy, E., Łangowski, Ł., Kleine-vehn, J., Fan, Y., Morita, M.T., Tasaka, M., Fankhauser, C., Offringa, R., and Friml, J. (2011). Light-mediated polarization of the PIN3 auxin transporter for the phototropic response in *Arabidopsis*. Nat. Cell Biol. **13**:447–452.

Ding, Y., Sun, T., Ao, K., Peng, Y., Zhang, Y., Li, X., and Zhang, Y. (2018). Opposite roles of salicylic acid receptors NPR1 and NPR3/NPR4 in transcriptional regulation of plant immunity. Cell **173**:1454–1467.e15.

Du, Y., Tejos, R., Beck, M., Himschoot, E., Li, H., Robatzek, S., Vanneste, S., and Friml, J. (2013). Salicylic acid interferes with clathrin-mediated endocytic protein trafficking. Proc. Natl. Acad. Sci. **110**:7946–7951.

Duggan, K.C., Walters, M.J., Musee, J., Harp, J.M., Kiefer, J.R., Oates, J.A., and Marnett, L.J. (2010). Molecular basis for cyclooxygenase inhibition by the non-steroidal anti-inflammatory drug naproxen. J. Biol. Chem. **285**:34950–34959.

Duggan, K.C., Hermanson, D.J., Musee, J., Prusakiewicz, J.J., Scheib, J.L., Carter, B.D., Banerjee, S., Oates, J.A., and Marnett,

L.J. (2011). (R)-Profens are substrate-selective inhibitors of endocannabinoid oxygenation by COX-2. Nat. Chem. Biol. **7**:803–809.

Emsley, P., Lohkamp, B., Scott, W.G., and Cowtan, K. (2010). Features and development of coot. Acta Crystallogr. D Biol. Crystallogr. **66**:486–501.

Friml, J. (2022). Fourteen stations of auxin. Cold Spring Harb. Perspect. Biol. **14**:a039859.

Friml, J., Wiśniewska, J., Benková, E., Mendgen, K., and Palme, K. (2002). Lateral relocation of auxin efflux regulator PIN3 mediates tropism in *Arabidopsis*. Nature **415**:806–809.

Friml, J., Vieten, A., Sauer, M., Weijers, D., Schwarz, H., Hamann, T., Offringa, R., and Jürgens, G. (2003). Efflux-dependent auxin gradients establish the apical-basal axis of *Arabidopsis*. Nature **426**:147–153.

Friml, J., Gallei, M., Gelová, Z., Johnson, A., Mazur, E., Monzer, A., Rodriguez, L., Roosjen, M., Verstraeten, I., Živanović, B.D., et al. (2022). ABP1-TMK auxin perception mediates ultrafast global phosphorylation and auxin canalization. Nature **609**:575–581.

Fu, Z.Q., Yan, S., Saleh, A., Wang, W., Ruble, J., Oka, N., Mohan, R., Spoel, S.H., Tada, Y., Zheng, N., and Dong, X. (2012). NPR3 and NPR4 are receptors for the immune signal salicylic acid in plants. Nature **486**:228–232.

Gallei, M., Luschnig, C., and Friml, J. (2020). Auxin signalling in growth: Schrödinger's cat out of the bag. Curr. Opin. Plant Biol. **53**:43–49.

Gälweiler, L., Guan, C., Müller, A., Wisman, E., Mendgen, K., Yephremov, A., and Palme, K. (1998). Regulation of polar auxin transport by AtPIN1 in *Arabidopsis* vascular tissue. Science **282**:2226–2230.

Hansen, H., and Grossmann, K. (2000). Auxin-induced ethylene triggers abscisic acid biosynthesis and growth inhibition. Plant Physiol. **124**:1437–1448.

Hao, P., Xia, J., Liu, J., Di Donato, M., Pakula, K., Bailly, A., Jasinski, M., and Geisler, M. (2020). Auxin-transporting ABC transporters are defined by a conserved D/E-P motif regulated by a prolylisomerase. J. Biol. Chem. **295**:13094–13105.

He, W., Brumos, J., Li, H., Ji, Y., Ke, M., Gong, X., Zeng, Q., Li, W., Zhang, X., An, F., et al. (2011). A small-molecule screen identifies l-kynurenine as a competitive inhibitor of TAA1/TAR activity in ethylene-directed auxin biosynthesis and root growth in *Arabidopsis*. Plant Cell **23**:3944–3960.

Huls, G., Koornstra, J.J., and Kleibeuker, J.H. (2003). Non-steroidal anti-inflammatory drugs and molecular carcinogenesis of colorectal carcinomas. Lancet **362**:230–232.

Ishihama, N., Choi, S.W., Noutoshi, Y., Saska, I., Asai, S., Takizawa, K., He, S.Y., Osada, H., and Shirasu, K. (2021). Oxicam-type non-steroidal anti-inflammatory drugs inhibit NPR1-mediated salicylic acid pathway. Nat. Commun. **12**:7303.

Ke, M., Ma, Z., Wang, D., Sun, Y., Wen, C., Huang, D., Chen, Z., Yang, L., Tan, S., Li, R., et al. (2021). Salicylic acid regulates PIN2 auxin transporter hyperclustering and root gravitropic growth via Remorin-dependent lipid nanodomain organisation in Arabidopsis thaliana. New Phytol. **229**:963–978.

Kleine-Vehn, J., Ding, Z., Jones, A.R., Tasaka, M., Morita, M.T., and Friml, J. (2010). Gravity-induced PIN transcytosis for polarization of auxin fluxes in gravity-sensing root cells. Proc. Natl. Acad. Sci. USA **107**:22344–22349.

Kong, M., Liu, X., Sun, L., and Tan, S. (2022). Molecular mechanisms of N-1 -naphthylphthalamic acid , a chemical tool in plant biology and agriculture. Mol. Hortic. **2**:22.

Konstantinova, N., Hörmayer, L., Glanc, M., Keshkeih, R., Tan, S., Di Donato, M., Retzer, K., Moulinier-Anzola, J., Schwihla, M., Korbei, B., et al. (2022). WAVY GROWTH Arabidopsis E3 ubiquitin ligases affect apical PIN sorting decisions. Nat. Commun. **13**:5147.

Ung, K.L., Winkler, M., Schulz, L., Kolb, M., Janacek, D.P., Dedic, E., Stokes, D.L., Hammes, U.Z., and Pedersen, P.B. (2022). Structures and mechanism of the plant PIN-FORMED auxin transporter. Nature **609**:605–610.

Lavy, M., and Estelle, M. (2016). Mechanisms of auxin signaling. Development **143**:3226–3229.

Li, L., Gallei, M., and Friml, J. (2022). Bending to auxin: fast acid growth for tropisms. Trends Plant Sci. **27**:440–449.

Liao, C.-Y., Smet, W., Brunoud, G., Yoshida, S., Vernoux, T., and Weijers, D. (2015). Reporters for sensitive and quantitative measurement of auxin response. Nat. Methods **12**:207–210, 2 p following 210.

Luschnig, C., Gaxiola, R.A., Grisafi, P., and Fink, G.R. (1998). EIR1, a root specific protein involved in auxin transport, is required for gravitropism in *Arabidopsis thaliana*. Genes Dev. **12**:2175–2187.

Marchant, A., Kargul, J., May, S.T., Muller, P., Delbarre, A., Perrot-Rechenmann, C., and Bennett, M.J. (1999). AUX1 regulates root gravitropism in Arabidopsis by facilitating auxin uptake within root apical tissues. EMBO J. **18**:2066–2073.

Nakamura, M., Nishimura, T., and Morita, M.T. (2019). Gravity sensing and signal conversion in plant gravitropism. J. Exp. Bot. **70**:3495–3506.

Nishimura, T., Hayashi, K.I., Suzuki, H., Gyohda, A., Takaoka, C., Sakaguchi, Y., Matsumoto, S., Kasahara, H., Sakai, T., Kato, J.I., et al. (2014). Yucasin is a potent inhibitor of YUCCA, a key enzyme in auxin biosynthesis. Plant J. **77**:352–366.

Okada, K., Ueda, J., Komaki, M.K., Bell, C.J., and Shimura, Y. (1991). Requirement of the auxin polar transport system in early stages of *Arabidopsis* floral bud formation. Plant Cell **3**:677–684.

Pasternak, T., Groot, E.P., Kazantsev, F.V., Teale, W., Omelyanchuk, N., Kovrizhnykh, V., Palme, K., and Mironova, V.V. (2019). Salicylic acid affects root meristem patterning via auxin distribution in a concentration-dependent manner. Plant Physiol. **180**:1725–1739.

Petrásek, J., Mravec, J., Bouchard, R., Blakeslee, J.J., Abas, M., Seifertová, D., Wiśniewska, J., Tadele, Z., Kubeš, M., Covanová, M., et al. (2006). PIN proteins perform a rate-limiting function in cellular auxin efflux. Science **312**:914–918.

Punjani, A., Rubinstein, J.L., Fleet, D.J., and Brubaker, M.A. (2017). CryoSPARC: algorithms for rapid unsupervised cryo-EM structure determination. Nat. Methods **14**:290–296.

Rakusová, H., Abbas, M., Han, H., Song, S., Robert, H.S., and Friml, J. (2016). Termination of shoot gravitropic responses by auxin feedback on PIN3 polarity. Curr. Biol. **26**:3026–3032.

Rong, D., Luo, N., Mollet, J.C., Liu, X., and Yang, Z. (2016). Salicylic acid regulates pollen tip growth through an NPR3/NPR4-independent pathway. Mol. Plant **9**:1478–1491.

Rosenthal, P.B., and Henderson, R. (2003). Optimal determination of particle orientation, absolute hand, and contrast loss in single-particle electron cryomicroscopy. J. Mol. Biol. **333**:721–745.

Salehin, M., Bagchi, R., and Estelle, M. (2015). SCF TIR1/AFB-based auxin perception: mechanism and role in plant growth and development. Plant Cell **27**:9–19.

Serrano, M., Wang, B., Aryal, B., Garcion, C., Abou-Mansour, E., Heck, S., Geisler, M., Mauch, F., Nawrath, C., and Métraux, J.P. (2013). Export of salicylic acid from the chloroplast requires the multidrug and toxin extrusion-like transporter EDS5. Plant Physiol. **162**:1815–1821.

Su, N., Zhu, A., Tao, X., Ding, Z.J., Chang, S., Ye, F., Zhang, Y., Zhao, C., Chen, Q., Wang, J., et al. (2022). Structures and mechanisms of the Arabidopsis auxin transporter PIN3. Nature **609**:616–621.

Tan, S. (2021). Action mode of NPA: direct inhibition on PIN auxin transporters. Mol. Plant **14**:199.

Tan, S., Zhang, X., Kong, W., Yang, X.L., Molnár, G., Vondráková, Z., Filepová, R., Petrášek, J., Friml, J., and Xue, H.W. (2020a). The lipid code-dependent phosphoswitch PDK1–D6PK activates PIN-mediated auxin efflux in Arabidopsis. Nat. Plants **6**:556–569.

Tan, S., Abas, M., Verstraeten, I., Glanc, M., Molnár, G., Hajný, J., Lasák, P., Petřík, I., Russinova, E., Petrášek, J., et al. (2020b). Salicylic Acid targets Protein Phosphatase 2A to attenuate growth in plants. Curr. Biol. **30**:381–395.e8.

Tan, S., Di Donato, M., Glanc, M., Zhang, X., Klíma, P., Liu, J., Bailly, A., Ferro, N., Petrášek, J., Geisler, M., and Friml, J. (2020c). Non-steroidal anti-inflammatory drugs target TWISTED DWARF1-regulated actin dynamics and auxin transport-mediated plant development. Cell Rep. **33**:108463.

Tan, S., Luschnig, C., and Friml, J. (2021). Pho-view of auxin: reversible protein phosphorylation in auxin biosynthesis, transport and signalling. Mol. Plant **14**:151–165.

Teale, W., and Palme, K. (2018). Naphthylphthalamic acid and the mechanism of polar auxin transport. J. Exp. Bot. **69**:303–312.

Teale, W.D., Pasternak, T., Dal Bosco, C., Dovzhenko, A., Kratzat, K., Bildl, W., Schwörer, M., Falk, T., Ruperti, B., Schaefer, J.V., et al. (2021). Flavonol-mediated stabilization of PIN efflux complexes regulates polar auxin transport. EMBO J. **40**:e104416.

Vandenbussche, F., Petrásek, J., Zádníková, P., Hoyerová, K., Pesek, B., Raz, V., Swarup, R., Bennett, M., Zazímalová, E., Benková, E., and Van Der Straeten, D. (2010). The auxin influx carriers AUX1 and LAX3 are involved in auxin-ethylene interactions during apical hook development in *Arabidopsis thaliana* seedlings. Development **137**:597–606.

Wang, W., Withers, J., Li, H., Zwack, P.J., Rusnac, D.V., Shi, H., Liu, L., Yan, S., Hinds, T.R., Guttman, M., et al. (2020). Structural basis of salicylic acid perception by *Arabidopsis* NPR proteins. Nature **586**:311–316.

Wu, Y., Zhang, D., Chu, J.Y., Boyle, P., Wang, Y., Brindle, I.D., De Luca, V., and Després, C. (2012). The *Arabidopsis* NPR1 protein is a receptor for the plant defense hormone salicylic acid. Cell Rep. **1**:639–647.

Xiao, Y., and Offringa, R. (2020). PDK1 regulates auxin transport and Arabidopsis vascular development through AGC1 kinase PAX. Nat. Plants **6**:544–555.

Yang, Z., Xia, J., Hong, J., Zhang, C., Wei, H., Ying, W., Sun, C., Sun, L., Mao, Y., Gao, Y., et al. (2022). Structural insights into auxin recognition and efflux by Arabidopsis PIN1. Nature **609**:611–615.

Yiannakopoulou, E. (2013). Pharmacogenomics of acetylsalicylic acid and other nonsteroidal anti-inflammatory agents: clinical implications. Eur. J. Clin. Pharmacol. **69**:1369–1373.

Yu, Z., Zhang, F., Friml, J., and Ding, Z. (2022). Auxin signaling: research advances over the past 30 years. J. Integr. Plant Biol. **64**:371–392.

Zádníková, P., Petrásek, J., Marhavy, P., Raz, V., Vandenbussche, F., Ding, Z., Schwarzerová, K., Morita, M.T., Tasaka, M., Hejátko, J., et al. (2010). Role of PIN-mediated auxin efflux in apical hook development of *Arabidopsis thaliana*. Development **137**:607–617.

Zhao, Y. (2018). Essential roles of local auxin biosynthesis in plant development and in adaptation to environmental changes. Annu. Rev. Plant Biol. **69**:417–435.

Zheng, S.Q., Palovcak, E., Armache, J.P., Verba, K.A., Cheng, Y., and Agard, D.A. (2017). MotionCor2: anisotropic correction of beam-induced motion for improved cryo-electron microscopy. Nat. Methods **14**:331–332.

Zivanov, J., Nakane, T., Forsberg, B.O., Kimanius, D., Hagen, W.J., Lindahl, E., and Scheres, S.H. (2018). New tools for automated high-resolution cryo-EM structure determination in RELION-3. Elife **7**:e42166.